Langmuir

Article

pubs.acs.org/Langmuir

Nucleation in Short-Range Attractive Colloids: Ordering and Symmetry of Clusters

Siddique J. Khan,† O. L. Weaver, C. M. Sorensen, and A. Chakrabarti*

Department of Physics, Kansas State University, Manhattan, Kansas 66503, United States

ABSTRACT: Results from extensive Brownian dynamics simulations are presented for nucleation in a system of colloidal particles interacting via a short-range attractive potential. Our analysis shows that, even though the system is not in equilibrium, structures of small size clusters compare well with the theoretically predicted and experimentally observed ground state structures for short-range colloidal systems. In addition, the distribution of the symmetric structures in nucleation is comparable to the distribution seen in equilibrium. We also investigate how the shape and structure of fluctuating clusters in the prenucleation regime affect the formation of a stable nucleating cluster.

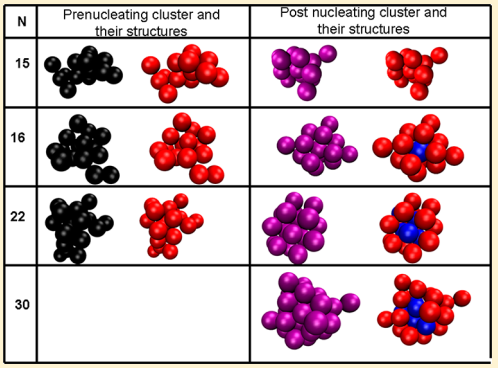

I. INTRODUCTION

A first step toward understanding the thermodynamics of the clustering process in short-range colloidal systems is to elucidate the equilibrium ground state morphology of small clusters. Such calculations are well established for long-range interaction potentials such as the Lennard-Jones potential.[1,2] More recently, a detailed study of the ground state equilibrium structure of a hard sphere system with a short-range interaction potential has been carried out.[3−5] A striking result[5] is that the presence of highly symmetric clusters is suppressed due to entropic reasons.

Once the morphology of equilibrium structures is well understood, the next step in our quest should involve studies of colloidal clusters in nonequilibrium, quenched systems. Thus, it is reasonable to ask how probable are symmetric structures during colloidal nucleation and whether the distribution of the symmetric structures in nucleation is similar to the distribution seen in equilibrium systems.[4,5] Additionally, one would like to investigate how the range of interaction affects the nucleation process of symmetric structures and whether the shape and structure of the fluctuating clusters in the prenucleation regime plays any notable role in the formation of a stable nucleating cluster.

We address these issues in this paper by carrying out extensive Brownian dynamics (BD) simulations of nucleation in a system of colloidal particles interacting via a short-range attractive potential. As a prototype for short-range interactions, we have chosen the Asakura-Oosawa-Vrij (AOV) potential,[6,7] which approximately accounts for the depletion interaction between a pair of colloidal particles by an effective two-body interaction. Once a system is quenched from a stable to a metastable regime, nucleation phenomena can be divided into two regimes: those that happen before a critical nucleus occurs (prenucleating regime) and those that happen after the critical nucleus forms (nucleating regime). A thorough analysis of the shape, morphology, and crystalline structure of clusters is made in both of these regimes for two different values for the depth and range of the interaction potential. Our work is more realistic to model homogeneous nucleation than recent studies[8] that numerically yield nonequilibrium clusters of high symmetry starting from a core seed.

II. SIMULATION METHOD

In our BD simulations,[9] we consider 3D systems of different linear sizes from $L = 128d$ to $L = 512d$ in units of monomer diameter d. All other length scales are measured in units of d as well. The equations of motion for the BD simulation read as

$$\ddot{\vec{r}}_i = -\nabla U_i - \Gamma\dot{\vec{r}}_i + W_i(t) \quad (1)$$

where Γ is the friction coefficient and W_i is the random force acting on each colloidal particle i, a Gaussian white noise satisfying fluctuation−dissipation relation. Hydrodynamic interactions, including lubrication forces, are ignored in the simulation as they might not be of predominant importance for a study of quiescent secondary minimum colloids.[10−12] The potential U acting upon each colloidal particle has a 2-fold contribution: the two-body depletion potential of AOV (U_{AO}) plus a repulsive hard-core-like interaction (U_{hc}) given by the following expressions:

$$U(r_{ij}) = U_{AO}(r_{ij}) + U_{hc}(r_{ij}) \quad (2)$$

where

Received: July 31, 2012
Revised: October 15, 2012
Published: October 16, 2012

$$\frac{U_{AO}}{kT} = \phi_p\left(\frac{1+\zeta}{\zeta}\right)^3\left[\frac{3r_{ij}}{2(1+\zeta)} - \frac{1}{2}\left(\frac{r_{ij}}{1+\zeta}\right)^3 - 1\right] \text{ for } r_{ij} < 1+\zeta \quad (3a)$$

$$=0 \text{ for } r_{ij} > 1+\zeta \quad (3b)$$

and

$$\frac{U_{hc}}{kT} = r_{ij}^{-\alpha} \quad (4)$$

In eq (3), ζ controls the range of the depletion interaction (r_c) in the AOV model such that $r_c = 1+\zeta$ and ϕ_p is a parameter that controls the strength of the interaction. Most of our simulations are for $\zeta = 0.05$ and 0.3, whereas some simulations have also been carried out for $\zeta = 0.8$.

In the hardcore-like repulsive interaction given by eq 4, we have set $\alpha = 36$. Exponents $\alpha < 36$ are reported to lead to anomalies when a hard-core mimic is required in the potential.[13] The total pair potential $U = U_{AO} + U_{hc}$ passes through a minimum value (U_{min}) that depends on ζ and ϕ_p. In what follows, we will often characterize the strength of the potential in terms of the absolute value of the minimum potential depth, $U_m = |U_{min}|$ rather than by ϕ_p. Table 1 lists the minimum potential depth and the values of various parameters used in the simulations. We choose $\Gamma = 0.5$ and time step $\Delta t = 0.005$ in reduced time units of $d(m/kT)^{1/2}$ with $m = 1$. For this choice of Γ, particle motion is purely diffusive for $t \gg 1/\Gamma$, that is, $t \gg 2$ in our units. Periodic boundary conditions are enforced to minimize wall effects. The volume fraction, f, is chosen small enough such that only one or few small clusters grow in the simulation box. All simulations start from a random initial monomer conformation and the results for the kinetics are averaged over many (100 in most cases) runs.

Table 1. Simulation Quench Depths (U_m), Number of Monomers (N_m), and Volume Fractions (f) for Different ζ Values

	U_m	N_m	f
$\zeta = 0.05$	4 kT	12 000	5×10^{-2}
	10 kT	1500	1.7×10^{-5}
$\zeta = 0.3$	3 kT	14 680	3.64×10^{-3}
	10 kT	1750	4×10^{-4}
$\zeta = 0.8$	4 kT	6000	1.86×10^{-4}

III. RESULTS

III.A. Dynamics of the Largest Cluster. To study the dynamics of the nucleation process for different ranges of interaction, we focus on the largest cluster present in the system at any time after an initial quench. Cluster growth dynamics for the short-range system ($\zeta = 0.05$) is shown in parts a and b of Figure 1, where it can be seen that the largest cluster in the system grows in mainly two ways. In type-1 growth (part a of Figure 1), frequent excursions in size take place in the prenucleation regime when the largest cluster is unstable followed by a sudden increase in size in the nucleation regime where a stable growing cluster is found. However, in type-2 growth (part b of Figure 1), there are no huge size fluctuations in the prenucleation regime and the cluster smoothly enters the nucleation regime. It should be noted that the time required to form a stable nucleating cluster in type-2 is much smaller as compared to the time required in type-1 system. This is due to the fact that more compact clusters are formed in type-2 dynamics and once formed they grow steadily. We find that type-1 dynamics occurs more frequently (more than 60% cases) as compared to the type-2 dynamics.

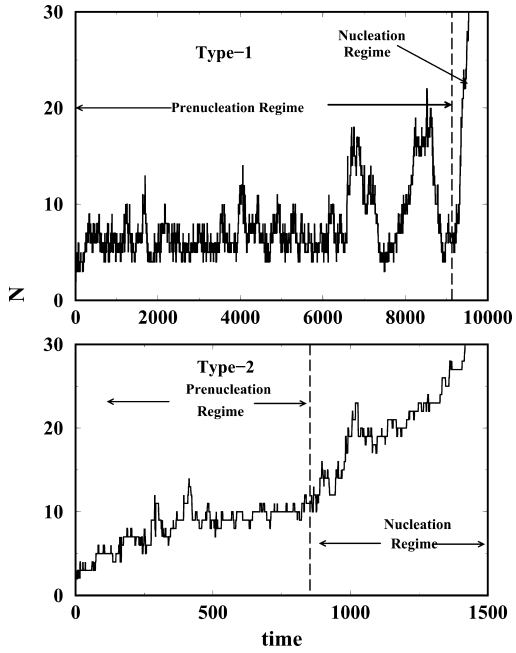

Figure 1. A plot showing two different types of size fluctuations during the dynamics of the largest cluster in the short-ranged system of $\zeta = 0.05$ with quench depth of $4kT$. In type-1 growth, one finds large number of excursions above the critical size (about $N = 10$) in the prenucleating regime, whereas in type-2 few such excursions are seen. Rather, a nucleating cluster is seen to grow monotonically to a stable size in this type of nucleation.

These fluctuations were also observed for a longer range system ($\zeta = 0.3$). The size variations, however, are not huge at $4kT$ quench depth (maximum excursion up to $N = 10$) and hence it becomes difficult to study the excursions in size for such small size clusters. So, for a better understanding of these size fluctuations, we have studied the nucleation mechanism at a quench depth of $3kT$ for the case of $\zeta = 0.3$. Here, the size fluctuations in the prenucleation regime are found to be up to $N = 40$, whereas the critical nucleus size is about 16. The cluster growth dynamics for this case also shows that the formation of the stable nucleating cluster mostly occurs through the type-1 dynamics.

III.B. Morphology of Clusters. To further investigate such complex dynamics, we compare and characterize the morphology and structure of clusters in the prenucleating and nucleating regimes by computing the radius of gyration R_g and cluster shape anisotropy (A_{13}) as a function of cluster size. Here, cluster shape anisotropy is defined as the ratio of the squares of the largest and smallest principle radii of gyration.[14] These results are shown in Figure 2. A fit to the data points in parts a and b of Figure 2 indicates that the clusters found in our simulations are compact as $N = \sim R_g^3$ for both prenucleation and nucleation regimes in both short-ranges and relatively long-ranged systems.[15] Also, from the cluster shape anisotropy studies calculations, shown in parts c and d of Figure 2, we can conclude that clusters in both prenucleating and nucleating regimes have almost identical shape morphology. The larger

dx.doi.org/10.1021/la303894s | Langmuir 2012, 28, 16015−16021

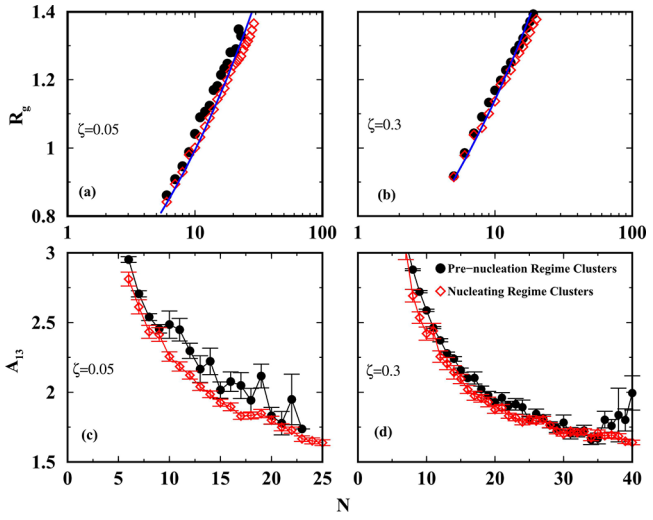

Figure 2. A plot showing the variation of the radius of gyration (R_g) and shape anisotropy (A_{13}) as a function of the size (N) for both ranges of ζ = 0.05 and 0.3 and quench depth of U_m = 4kT and 3kT, respectively. (a and b) show the variation of the R_g indicating a compact morphology of the clusters in both cases; (c and d) describe the variation of the shape anisotropy parameter A_{13} as a function of the size indicating that the clusters in both regimes have almost identical shape morphology although the prenucleation regime clusters have larger error bars.

error bars for the prenucleation regime clusters arise from the large fluctuation in shape for these clusters.

III.C. Energetics of Clusters. Next, we calculate and compare the averaged energy $\langle E\rangle$ per particle (N) of the clusters in both prenucleating and nucleating regimes. This comparison is shown in parts a and b of Figures 3. It is clear

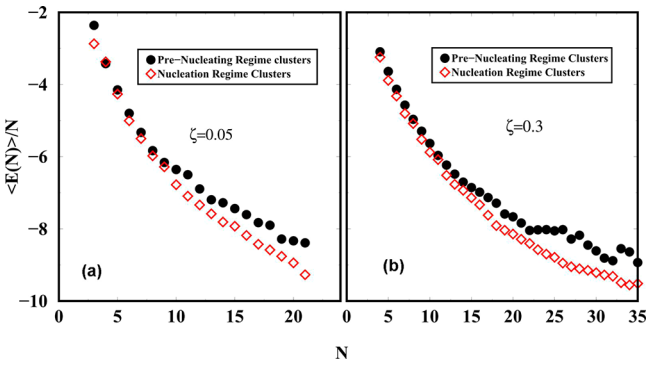

Figure 3. (a) Comparison of energy per particle $\langle E\rangle$ as a function of the size N for both prenucleating and nucleation regime clusters. In this case, ζ = 0.05 and the quench depth is 4kT. The nucleating clusters are energetically more stable as compared to the prenucleating clusters above a critical value of size N. From the bifurcation in energy we estimate the critical size of the clusters to be $N \approx 10$. (b) Same as (a) except for ζ = 0.3 and the quench depth is 3kT. In this case, we estimate the critical size of the clusters to be $N \approx 16$.

that the nucleating regime clusters have lower energy $\langle E\rangle/N$ compared to prenucleating regime clusters for sizes above a critical value where the two curves tend to separate from each other. This bifurcation in energies provides a good measure for the critical size of the nucleating cluster.

III.D. Crystalline Nature of Clusters. From our results so far, we have been able to establish the fact that, in the case of a short-range attractive colloidal system, clusters in the nucleating regime have lower energy than clusters in prenucleating regime, even though clusters in both regimes are compact and have similar shape morphology as described by A_{13}. The next step in our study must then be to probe the symmetry and crystallinity of these clusters. To study the local crystallinity of particles a cluster, we compute a quantity called $q_6(i).q_6(j)$ based on the Steinhardt bond order parameters.[16−18] These parameters are written in terms of the spherical harmonics. For a particle i in the cluster with $N_b(i)$ neighboring particles, one defines a bond orientation order parameter

$$\bar{q}_{lm}(i) = \frac{1}{N_b(i)} \sum_{j=1}^{N_b(i)} Y_{lm}(\vec{r}_{ij}) \tag{5}$$

where $Y_{lm}(\vec{r}_{ij})$ are the spherical harmonics related to the orientation of the jth neighboring particle of the particle i. Our analysis is done using l = 6 because most of the common crystalline structures have distinctive values at l = 6. A vector $q_6(i)$ is defined for each particle as

$$q_{l=6}(i) \equiv \left[\frac{4\pi}{2l+1} \sum_{m=-l}^{l} |\bar{q}_{lm}(i)|^2\right]^{1/2} \tag{6}$$

and a scalar product is next taken with the corresponding vectors of the neighboring particles $N_b(i)$ to define:

$$q_6(i).\, q_6(j) = \sum_{m=-6}^{6} q_{6m}(i) q^*_{6m}(j) \tag{7}$$

If this scalar product for any two neighboring particles is greater than a threshold value of 0.7,[19] the particles are regarded as the connected and a particle with more than 8 connections is considered a crystalline particle. Furthermore, distinction between different crystalline structures is made by using the definition mentioned in ref 20. Because the number of crystalline particles N_c fluctuates with time in both prenucleating and nucleating regimes, we calculate the average number of crystalline particles $\langle N_c\rangle$ in a given size cluster. A comparison of this quantity $\langle N_c\rangle$ between clusters in these two regimes is shown in parts a and b of Figure 4. It is clear from parts a and b of Figure 4 that clusters in the prenucleating regime have none or very few crystalline particles. In the nucleation regime for a very short-range system with ζ = 0.05, clusters show a significant rise in $\langle N_c\rangle$ once their size is more than 15.

A comparison of the crystalline nature of prenucleating and nucleating regime clusters are next directly shown in Figure 5 by taking different snapshots of the largest cluster in the system from both regimes. On the left column, snapshots of the prenucleating cluster are shown at different sizes, whereas on the middle column nucleation regime clusters with same size are shown. The right column shows the nucleation regime clusters with developing crystalline structure (shown in green color). The observed crystalline order is based on the bond-order parameter. This comparison shows that no crystalline order is present in the prenucleation regime clusters, whereas nucleating clusters show significant presence of developing crystalline structure.

The formation of the crystalline structure in the nucleating regime cluster indicates that crystallization plays an important role in the nucleation mechanism of the short-range interaction

dx.doi.org/10.1021/la303894s | Langmuir 2012, 28, 16015−16021

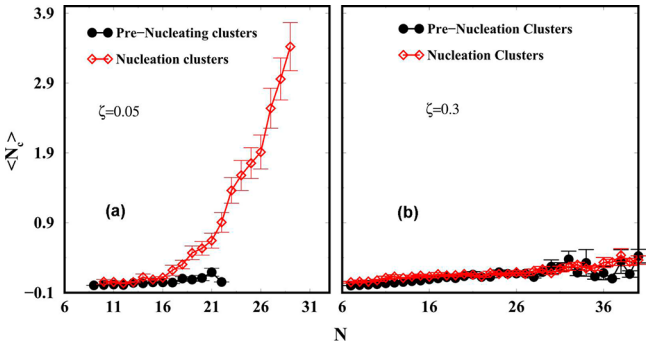

Figure 4. Plot showing the variation in the number of crystalline particles N_c (averaged over 100 runs) as a function of the cluster size N for both nucleating and prenucleating regime clusters. The averaged number of crystalline particles $\langle N_c \rangle$, defined in text, remains almost zero in prenucleating regimes. For the case of short-range potential (i.e., $\zeta = 0.05$ and $U_m = 4kT$), a significant rise in $\langle N_c \rangle$ is observed in nucleating regime for $N > 15$ as shown in (a). However, (b) shows that no crystalline structure seems to exist for clusters even in the nucleating regime in the case of longer interparticle range $\zeta = 0.3$ and quench depth of $3kT$.

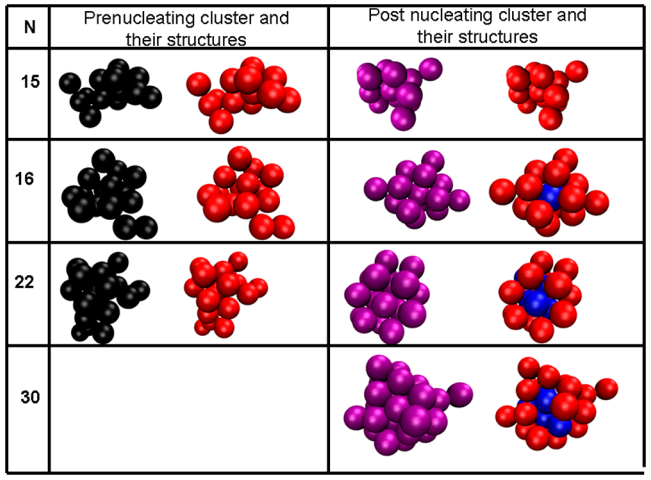

Figure 5. Comparison of the crystalline structure between the prenucleating and nucleation regime clusters (taken from the simulation run shown in part a of Figure 1) of a given size N for $\zeta = 0.05$ and $U_m = 4kT$ potential depth is shown here. The red color in this picture is indicator of liquidlike structure and blue color represents the crystalline structure. The left column shows the prenucleating clusters (black color) of a given size N and their liquidlike structures (shown in red color). The right column shows the nucleating regime clusters (purple color) of the corresponding sizes and their structure showing the presence of crystalline particles in the nucleating clusters surrounded by liquidlike particles. It should be noted that no crystalline structure is observed in the prenucleating clusters (there is no prenucleation regime cluster found for $N = 30$ in that run), whereas nucleating regime clusters show the developing crystalline structure after $N = 15$ ($N_c = 0$ is observed for $N = 15$ in the postnucleation regime) indicated by crystalline particles N_c (shown in blue color) surrounded by the liquidlike particles.

colloidal system and only those clusters with crystalline order in their structure grow out to a stable size.

However, no crystalline structure is found in nucleating clusters for the case of longer interation range, that is, $\zeta = 0.3$. This can be understood from the phase diagram computed in the literature for the AOV model.[21,22] Locations for quenches considered in this study are in the fluid−solid coexistence region for $\zeta = 0.05$, whereas quench points are located inside the metastable fluid−fluid coexistence region for $\zeta = 0.3$. Although the fluid−fluid coexistence is metastable for $\zeta = 0.3$ it seems to influence the crystallinity of the growing cluster. Our further analysis shows that even after forming a stable size cluster, the structure of the nucleating cluster is found to remain liquidlike in this case until it reaches a reasonable size of $N = \sim 100$. This observation of liquidlike structure of small size nucleating clusters is consistent with our recent study of long-range interparticle interaction system of ligated gold nanoparticles[16] and with earlier expectations in the literature.[23]

III.E. Distribution of Symmetric Structures. In both prenucleating and nucleating regimes, various small sized clusters grow and disappear in the bulk. In this section, we study the symmetry of these small sized clusters. As mentioned before, a recent study of the ground-state equilibrium structure of a hard sphere system with a short-range interaction potential shows that the number of highly symmetric clusters is very low due to entropic reasons. In addition, the experimentally measured distribution of the clusters is found to be comparable with the theoretically calculated distribution for a system of hard spheres.[24] Whether such entropic effects play a predominant role for colloidal nucleation is an open question. For example, one would like to know the distribution of symmetric structures in nucleation and compare this distribution to the equilibrium distribution of such structures. As we are interested in comparison with theory and experiment, we focus on the shorter range model.

To accurately identify the symmetric structures one needs to work with a fixed value of nearest neighbor distance (bond length) between monomers. Thermal effects often lead to a fluctuation of the bond length and identification of symmetric structures become extremely difficult. To reduce the thermal effects on bond lengths, we consider $U_m = 10kT$ in this section. The monomer volume fraction is also lowered appropriately such that only one or few isolated clusters grow in the system. In this case, the size of the critical nucleus is very small (2 or 3 monomers) and thus most of our results are for the nucleating regime.

We accumulated clusters of different sizes at different times as they grow and dissolve in the system and classified them based on the number of contacts, C, present in the cluster. A list of maximum number of contacts (C_{max}) is shown in Table 2 for a short-range system with $\zeta = 0.05$ and compared with the theoretically calculated values of C_{max} using the concept of minimally rigid packing of spheres; for details about the packing of spheres, ref 24. For example, for a cluster of size $N = 6$, there can be a minimum of 5 and maximum of 12 possible contacts. In an ensemble of clusters of size $N = 6$, one would thus see a distribution of contacts from minimum of $C_{min} = 5$ to the maximum of $C_{max} = 12$. After selecting the clusters at different times during the nucleation process, we filter out and keep only clusters with maximum number of contacts (for example, 12 contact clusters for $N = 6$). On the basis of the finite sphere packing calculations,[3] there are two possible structures (octahedron and polytetrahedron) with maximum number of contacts ($C_{max} = 12$) for $N = 6$ size clusters. The presence of these two structures can be observed based on the moment of inertia (MOI) (I) and symmetry number (σ) calculations.

Note that σ is defined as rotational symmetry number which is calculated by applying different point group operations (also known as symmetry operations) on the cluster. For example, a six size cluster ($N = 6$) contains two symmetry structures (i.e.,

dx.doi.org/10.1021/la303894s | Langmuir 2012, 28, 16015−16021

Table 2. Comparison of Maximum Number of Contacts for Our Simulation Clusters with Ground State Clusters with a Short Range Interaction System,[5] Results for a Long-Range Interaction (Lennard-Jones) System Are Also Given.[29]

n	C_{max} for short-range intercation	C_{max} in our system for ζ = 0.05	C_{max} for LJ interaction
3	$3n - 6$	$3n - 6$	$3n - 6$
4	$3n - 6$	$3n - 6$	$3n - 6$
5	$3n - 6$	$3n - 6$	$3n - 6$
6	$3n - 6$	$3n - 6$	$3n - 6$
7	$3n - 6$	$3n - 5$	$3n - 5$
8	$3n - 6$	$3n - 5$	$3n - 5$
9	$3n - 6$	$3n - 4$	$3n - 4$
10	$3n - 5$	$3n - 4$	$3n - 3$
11	$3n - 4$	$3n - 3$	$3n - 2$
12	$3n - 3$	$3n - 3$	$3n$
13	$3n - 3$	$3n - 2$	$3n + 3$
14	$3n - 2$	$3n - 1$	$3n + 3$
15	$3n - 1$	$3n - 1$	$3n + 3$

octahedron and polytetragonal). Applying the point group operation, we find that polytetragonal structure has C_{2v} symmetry (in Schoenflies notation), which corresponds to σ = 2. Similarly, octahedron is found to have O_h symmetry in the same notation which corresponds to σ = 24.

The most symmetric structures will have lower I value and higher symmetry number value as compared to the one with less symmetric structure. These two parameters are also related through the rotational partition function (i.e., $Z_{rot} \approx \sqrt{I/\sigma}$). So the smaller values of Z_{rot} will represent the more symmetric structures in the system. As Meng et al.[5] have shown that rotational entropy makes the largest contribution to the free energy difference between the two structures in equilibrium, our analysis focuses on these two parameters; I and σ.

For small size clusters (i.e., N = 3,4,5), moment of inertia calculations show that there is only one ground state structure with maximum number of contacts present in the system, an observation consistent with the experiment and theory mentioned in ref 5. For larger sized clusters, starting at N = 6, we do compute both MOI and σ.

For the calculations of symmetry numbers,[25] we make use of an algorithm mentioned in ref 26. Because our clusters, being in the bulk, are not in equilibrium with the environment, it is difficult to achieve the exact value of the symmetry numbers for a given cluster with higher symmetry numbers. For example, for the case of octahedron structure, O_h, the exact value of symmetry number is σ = 24 and, for polytetrahedron structure, the symmetry number is σ = 2. In our simulations, we observe a broad distribution of symmetry numbers ranging from these two limiting values of σ = 2 to σ = 24 as shown in the Figure 6. The calculations of the symmetry number (σ) are very sensitive to the positions of the monomers and to small fluctuation of the bond length due to thermal effects. Even with these limitations, we clearly observe that the less symmetric structure is predominant among these maximum-contact clusters.

Most symmetric structures will have lower values of moment of inertia (MOI).[27] The MOI distribution shown in Figure 7 supports the conclusion drawn from the distribution of the symmetry numbers in Figure 6. One clearly finds from Figure 7 that the most symmetric ones occur less frequently as compared to the less symmetric ones. The less symmetric structure of polytetrahedron appears approximately 25−30

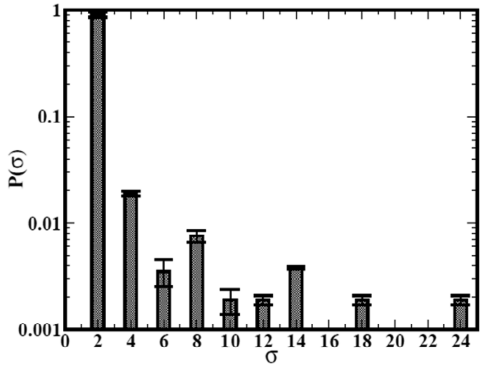

Figure 6. Semilog plot of the distribution of symmetry numbers calculated for N = 6 size clusters with C_{max} = 12 for short-range system with ζ = 0.05 and quench depth of U_m = 10kT. The results are averaged over 20 different runs.

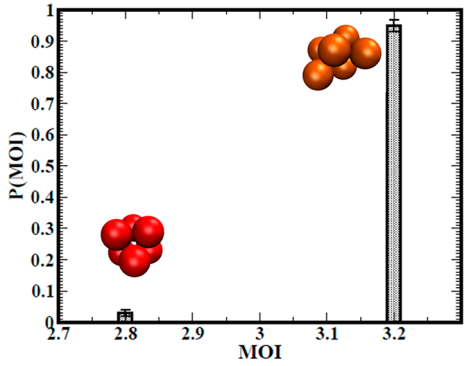

Figure 7. Plot of the moment of inertia (MOI) distribution of N = 6 clusters in the short-range system with ζ = 0.05 and quench depth of U_m = 10kT. Less symmetric structure polytetrahedron (brown structure) is found to appear 20 times more frequently as compared to more symmetric structure of octahedron (red structure). The results are averaged over 20 different runs.

times more frequently as compared to the most symmetric octahedron structure, even though both structures have the exact same energy (as both have the exact same number of contacts).

Another parameter of interest is the so-called $W_6(i)$ parameter based on the measurement of the local bond order parameters defined earlier in section III.D. This parameter describes the order of the neighbors around each particle in the cluster and is defined as follows:

$$\hat{w}_l(i) \equiv w_l(i)/[\sum_{m=-l}^{l} |q_{lm}(i)|^2]^{3/2} \quad (8)$$

$$w_l(i) = \sum_{\substack{m_1,m_2,m_3 \\ m_1+m_2+m_3=0}} \begin{pmatrix} lll \\ m_1 m_2 m_3 \end{pmatrix} \times q_{lm_1}(i) q_{lm_2}(i) q_{lm_3}(i) \quad (9)$$

Each structure has unique value of W_6 parameter,[28] which we calculate by first computing $W_6(i)$ for each particle i and then averaging over all the particles in the cluster. Distribution of $W_6(i)$ shown in Figure 8 strongly supports conclusions drawn from Figure 7 based on the distribution of MOI.

For larger sized clusters, the number of ground state structures increases with minor differences in their moment of inertia values, and it becomes difficult to distinguish these

dx.doi.org/10.1021/la303894s | Langmuir 2012, 28, 16015−16021

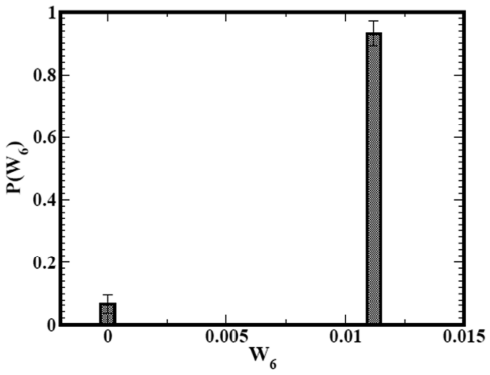

Figure 8. Plot of the W_6 distribution showing the comparative appearance of octahedron and polytetrahedron structures in the system. W_6 = 0.0 is indicative of the appearance of the octahedron while W_6 = 0.013 indicates the formation of polytetrahedron. This distribution is plotted for the short-range system with ζ = 0.05 and quench depth of U_m = 10kT. The results presented are averaged over 20 different runs.

structures based on an MOI distribution analysis. But based on the symmetry number calculations, we can still identify the frequency of most symmetric structures for N = 7 and N = 8. Figure 9 shows our results for such an analysis. We find that the

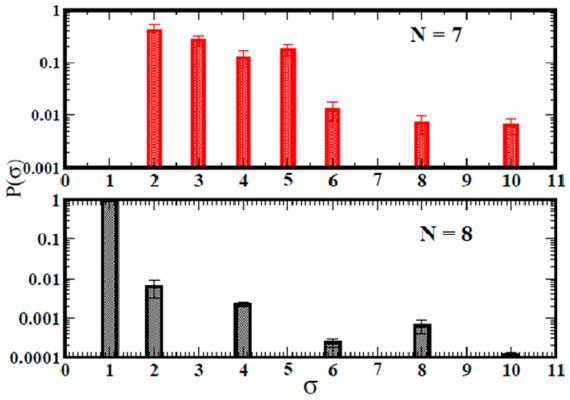

Figure 9. Plot of the distribution of symmetry numbers calculated for N = 7 and N = 8 with maximum number of contacts for ζ = 0.05 and quench depth of U_m = 10kT. About 1% presence of the most symmetric structure (D_{5h} with σ = 10) for the N = 7 and appearance of no symmetric structures of T_d (with σ = 12) and negligible appearance of D_{3d} (with σ = 6) and D_{2d} (with σ = 4) for N = 8 in the sample is surprisingly similar to the experimental observations mentioned in the text.

frequency of the most symmetric structure agrees well with theoretical and experimentally observed values.[5] For the case of N = 7, the most symmetric structure is D_{5h} (with σ = 10), and we find the frequency of this structure is 3.12%, which compares well to the theoretical value of 2.83% (experimentally, these structures cannot be distinguished from C_{2v} (with σ = 2) structures so the experimental values are unknown). For N = 8, we did not find any presence of the highly symmetric structures of T_d (with σ = 12), and D_{3d} (with σ = 6) which seems puzzling until we note that a similar null conclusion was reached by Meng et al. from their experiments.

IV. SUMMARY AND CONCLUSIONS

We have carried out detailed Brownian dynamics simulations to study nucleation in attractive colloidal systems. To distinguish between prenucleating and nucleating regimes, we have looked at the dynamics of the largest cluster in the simulation box. One can do a systematic study of computing the size of the critical cluster in terms of the supersaturation as described in our previous work.[16] However, our main focus in this current article is different and for this reason we have decided to define the line separating the prenucleating and nucleating regimes somewhat qualitatively. In the prenucleation regime, the largest cluster is not necessarily the same cluster that grows throughout this regime; rather one cluster can grow up to certain size and decay back and a new cluster can start developing in some other region of the box. However, for the volume fraction considered here, only one stable cluster grows in our finite sized simulation box in the nucleating regime. In this regime, growth of the same largest cluster takes place with the addition (and occasional subtraction) of monomers/dimers.

For the case of a short-range interacting system, our analysis of prenucleation and nucleation regime clusters suggests that nucleating clusters are not only energetically more stable but also carry signature of crystalline order. For the case of relatively long-ranged interacting system, the nucleating cluster is also energetically more stable as compared to prenucleating clusters of similar sizes. However, no crystalline structure is found to contribute to the formation of a stable nucleating cluster in this case. The nucleating cluster is liquidlike in this case until it grows up to a size significantly larger than the critical nucleus size. This can be understood from the location of the quench points with respect to the phase diagram computed in the literature for the AOV model.[21,22] Although the fluid−fluid coexistence is metastable, the proximity of the quench location to this coexistence seems to influence the crystallinity of the growing cluster.

One main purpose of this study is to check whether the distribution of symmetric structures seen at equilibrium appears in nucleation. Our analysis of moment of inertia and symmetry number of clusters shows that, even though the system is not in equilibrium, structures of small size clusters compare well with the theoretically predicted and experimentally observed ground state structures for short-range colloidal systems. In addition, the distribution of the symmetric structures in nucleation is comparable to the distribution seen in equilibrium.

AUTHOR INFORMATION

Corresponding Author

*E-mail: amitc@phys.ksu.edu.

Present Address

†Department of Biomedical Engineering, Washington University in St. Louis, St. Louis, MO 63130.

Notes

The authors declare no competing financial interest.

ACKNOWLEDGMENTS

This work was supported by NSF NIRT grant CTS0609318.

REFERENCES

(1) Freeman, D. L.; Doll, J. D. Computational Studies of Clusters: Methods and Results. *Annu. Rev. Phys. Chem.* **1996**, *47*, 43.

(2) Haore, M. R. Structure and Dynamics of Simple Microclusters. *Adv. Chem. Phys.* **2007**, *40*, 49−135.

(3) Arkus, N.; Manoharam, V. N.; Brenner, M. P. Minimum Energy Clusters of Hard Spheres with Short Range Attractions. *Phys. Rev. Lett.* **2009**, *103*, 118303.
(4) Hoy, R. S.; Harwayne-Gidansky, J.; O'Hern, C. S. Structure of finite sphere packings via exact enumerations: Implications for colloidal crystal nucleation. *Phys. Rev. E* **2012**, *85*, 051403.
(5) Meng, G.; Arkus, N.; Brenner, M. P.; Manoharan, V. N. The Free-Energy Landscape of Clusters of Attractive Hard Spheres. *Science* **2010**, *327*, 560.
(6) S. Asakura, S.; Oosawa, F. Surface Tension of High-Polymer Solutions. *J. Chem. Phys.* **1954**, *22*, 1255.
(7) Vrij, A. Polymers at interfaces and the interaction in Colloidal Dispersions. *Pure Appl. Chem.* **1976**, *48*, 471.
(8) Gorshkov, V.; Zavalov, A.; Privman, V. Shape Selection in Diffusive Growth of Colloids and Nanoparticles. *Langmuir* **2009**, *25*, 7940−7953.
(9) Gunsteren, W. F.; Berendsen, H. J. Algorithms for Brownian Dynamics. *Mol. Phys.* **1982**, *45*, 637.
(10) Nguyen, N. Q.; Ladd, A. J. C. Lubrication Corrections for Lattice-Boltzmann Simulations of Particle Suspensions. *Phys. Rev. E* **2002**, *66*, 046708.
(11) Brady, J. F. The Rheological Behavior of Concentrated Colloidal Dispersions. *J. Chem. Phys.* **1993**, *99*, 567.
(12) Riese, D. O.; Wegdam, G. H.; Vos, W. L.; Sprik, R.; Fenistein, D.; Bongaerts, J. H. H.; Grubel, G. Effective Screening of Hydrodynamic Interactions in Charged Colloidal Suspensions. *Phys. Rev. Lett.* **2000**, *85*, 5460.
(13) Melrose, J. R. Aggregate Network under Shear. *Europhys. Lett.* **1992**, *19*, 51.
(14) Fry, D.; Mohammad, A.; Chakrabarti, A.; Sorensen, C. M. Cluster Shape Anisotropy in Irreversible Aggregating Particulate Systems. *Langmuir* **2004**, *20*, 7871−7879.
(15) On the contrary, for the case of ligated gold nanoparticle system, our recent simulation study[16] (where the range of interaction is large as compared to the systems studied here) shows that the small size prenucleating clusters can be well described by self-avoiding random walk on a fcc lattice.
(16) Khan, S. J.; Sorensen, C. M.; Chakrabarti, A. Computer Simulations of Nucleation of Nanoparticles from Solutions. *Langmuir* **2012**, *28*, 5570−5579.
(17) Steinhardt, P. J.; Nelson, D. R.; Ronchetti, M. Bond-Orientational Order in Liquids and Glasses. *Phys. Rev. B* **1983**, *28*, 784−805.
(18) Auer, S.; Frenkel, D. Numerical Simulations of Crystal Nucleation in Colloids. *Adv. Polym. Sci.* **2005**, *173*, 149−207.
(19) Schilling, T.; Schope, H. J.; Oettel, M.; Opletal, G.; Snook, I. Precursor-Mediated Crystallization Process in Suspensions of Hard Spheres. *Phys. Rev. Lett.* **2010**, *105*, 025701.
(20) Desgranges, C.; Delhommelle, J. Polymorph Selection during the Crystallization of Softly Repulsive Spheres: The Inverse Power Law Potential. *J. Phys. Chem. B* **2007**, *111*, 12257−12262.
(21) Dijkstra, M.; van Roij, R.; Evans, R. Phase Behavior and Structure of Binary Hard-Sphere Mixtures. *Phys. Rev. Lett.* **1998**, *81*, 2268−2271.
(22) Dijkstra, M.; Brader, J. M.; Evans, R. Phase Behavior and Structure of Model Colloid-Polymer Mixtures. *J. Phys.:Condens. Matter* **1999**, *11*, 10079−10106.
(23) For example, see a review by Privman, V. In *Complex-Shaped Metal Nanoparticles*; Rogach, A. L., Sau, T. K., Eds.; Wiley-VCH, 2012; p 239.
(24) Arkus, N. *Theoretical Approaches to Self-Assembly and Biology*, PhD thesis, Applied Mathematics, Harvard University, Cambridge, MA, 2009.
(25) Falicov, L. M. *Group Theory and Its Physical Applications*, The University of Chicago Press, 1966.
(26) Cole, J. C.; Yao, J. W.; Shields, G. P.; Motherwell, W. D.; Allen, F. H.; Howard, J. A. Automatic Detection of Molecular Symmetry in the Cambridge Structural Database. *Acta Crystallogr.* **2001**, *B57*, 88−94.
(27) Vinothan, N.; Manoharan, V. N.; Elsesser, M. T.; Pine, D. J. Dense Packing and Symmetry in Small Clusters of Microspheres. *Science* **2003**, *301*, 483.
(28) Royall, C. P.; Williams, S. R.; Ohtsuka, T.; Tanaka, H. Direct Observation of a Local Structural Mechanism for Dynamic Arrest. *Nat. Mater.* **2008**, *7*, 556.
(29) Wales, D. J., Doye, J. P. K., Dullweber, A., Hodges, M. P., Naumkin, F. Y., Calvo, F., Hernandez-Rojas, J., Middleston, T. F.; *Cambridge Cluster Database*, http://physchem.ox.ac.uk/~doye/jon/structures/LJ.html